Biointerface Research in Applied Chemistry
Open-Access Journal (ISSN: 2069-5837)

Article
Volume 15, Issue 4, 2025, 54
https://doi.org/10.33263/BRIAC154.054

Surface Chemistry of Apatite at a Specific Concentration of 0.1 g/L: Phosphate Mineral

Mariam Khalil [1,*], Fatima Ezzahra Maarouf [1], Hind Khalil [1], Abdelkebir Bellaouchou [2], Saidati Bouhlassa [1], M'hamed Hmamou [1]

[1] Laboratory of Applied Chemistry of Materials (LCAM), Faculty of Sciences, Mohammed V University in Rabat, Morocco
[2] Laboratory of Materials, Nanotechnology and Environment, Mohammed V University, Faculty of Sciences, PO. Box. 1014, Rabat, Morocco
* Correspondence: mariamkhalil47@gmail.com;

Received: 7.11.2024; Accepted: 2.07.2025; Published: 9.08.2025

Abstract: The importance of the effect of phosphate rock depends on the chemical form of phosphorus in which this element is combined. ΔpH=f(pH) curves of the phosphate system measured for different hydration durations have a common intersection point that corresponds to the IEPs. The point of zero charges (PZC) and isoelectric point (IEP) were defined using the derivative method, examining the variations at lower contact times. The various parameters, such as pH, coexisting ions, concentrations of suspensions, and contact time, which govern the interfacial chemistry and interaction pathways, are discussed to understand the adsorption process. The experimental shift in PZC observed at a short hydration is controlled by a surface dipole moment of this structure induced by the charge redistributions of adsorbed water molecules. During hydration, strong columbic interactions of water are occurring with the calcium and the phosphate ions of the apatite surface.

Keywords: phosphate rock; surface chemistry; zero charges Pzc; isoelectric point IEP.

1. Introduction

The phosphate ore minerals are of a complex mineralogy, containing impurities that affect their surface chemistry. As a result, the surface chemistry of this phosphate ore is focused on the presence of Ca^{2+} and Mg^{2+} and on the mechanism of Al^{3+} and Fe^{3+} ions, which remains to be defined [1-4]. In general, the phosphate ore is a calcio-phosphate concentrate with around 35-38% P_2O_5 and 3-4% fluorine. The main sources of phosphate rock are fluorapatite with the general formula $Ca_{10}(PO_4)_6F_2$ [5-7]. The changes in the Ca/P ratio have a significant impact on the physical and chemical properties of HAP. This results in irregular structures and alters the organization of atoms within the crystal matrix [8,9]. There f core, these defects are associated with surface chemistry exchange that is crucial for the behavior of hydroxyapatite suspensions. The apatite ($Ca_5(PO_4)_3(X)$, X=OH, F), HAP, crystallizes in the hexagonal structure, and is usually expressed as $Ca_{10}(PO_4)_6(X)_2$, suggesting that the crystal unit encloses two molecular units. In these unit cells, there are 10 Ca^{2+} ions located in two distinct sites, denoted Ca(I) (four sites) and Ca (II) (six sites). The framework of HAP is described as a group of tetrahedral PO_4 ions, in which each tetrahedron is shared by one column and defines two kinds of unconnected channels. The first channel with a diameter of 2.5 Å is surrounded by Ca(I) sites. The second

type of channel, having 3.5 Å in diameter, is delimited by oxygen and Ca (II) ions. These channels are hosting hydroxyl/fluoride groups along the c-axis to balance the positive charge of the matrix. The hydroxyl anions are located in columns perpendicular to the unit cell surface, at the center of the hexagon made with coplanar Ca (II) groups. The oxygen atoms of the phosphate groups are labeled O(1), O(2), and O(3), and one of the hydroxyl groups is O(4). Two and four non-equivalent calcium and oxygen sites are shown in HAP, respectively. The Ca $(II)^{2+}$ columns are surrounded by O(1) and O(2) from PO_4^{3-} groups, while mirror-symmetric O(3) sites and Ca(II) cations are arranged in a hexagonal channel lodging the OH anions. The columnar Ca(I) cation is coordinated to six oxygen atoms of six different $(PO_4)^{3-}$groups, and to three oxygen atoms at a larger distance. The Ca(II) is found in cavities in the walls of the channels shaped between the calcium and oxygen atoms. This calcium is surrounded by six oxygen atoms of five different $(PO_4)^{3-}$and one OH group. The different HAP phases result in several alignments of OH in the hydroxyl channels. The hexagonal disordered phase is characterized by random orientations of OH ions, while in the hexagonal ordered phase, OH groups are all oriented along the same direction. Phosphate anions are the skeleton of the unit cell, arranged in two channels A and B along the c-axis. In the two channels A, the oxygen atoms from the phosphate groups and the Ca(II) ions are located at heights of 1/4 and 3/4, respectively. The two channels B contain Ca(I) cations, each at heights 0 and 1/2. So, the HAP molecular unit cell is rearranged as $Ca(I)_4Ca(II)(PO_4)_6(X)$, characterized by a three-dimensional network of hexagonally packed PO_4^{3-} tetrahedral, and one hydroxyl anion. These weakly bonded Ca sites are the main host sites of divalent impurities. Phosphate tetrahedra (six in total) are arranged in helices from heights z=0.25 to z=0.75. The six strongly bonded PO_4 anions and the half-occupied OH channel are aligned along the c-axis. The Ca(I) is relatively symmetric compared to the Ca(II). The distribution of impurity ions between these two calcium sites results in important variation in their physical characters [10]. The two channels along the c unit-cell axis, dispossessed of PO_4 ions, are filled by two Ca(I) ions at levels z = 0 and z = 0.5. Furthermore, it seems that the interaction between Ca(I) atoms is very low or does not exist, and this interaction is mostly prevailing between Ca(II) atoms and hydroxyl oxygen. The interaction, including oxygen from PO_4^-groups via Ca(II)-O(3)-Ca(I) channel, is also found to be insignificant. In this structure, calcium ions are in two different sites: four Ca(1) coordinated to nine oxygen atoms of six different $(PO_4)^{3-}$groups and six Ca(2) coordinated to six oxygen atoms of five different $(PO_4)^{3-}$ groups. Oxygen atoms of $(PO_4)^{3-}$groups are in three non-equivalent groups, and six Ca(2) coordinated to six oxygen atoms of five different $(PO_4)^{3-}$ groups. Oxygen atoms of $(PO_4)^{3-}$ groups are in three non-equivalent positions. The six Ca(II) atoms form a double triangle, placed between Ca(I) triangles, one set to z = 0.25 and the other to 0.75, leading to a hexagonal-axis tunnel (tunnel II). These calcium atoms are seven-fold coordinated to six oxygen atoms of the phosphate groups O(3) and one oxygen of the hydroxyl groups, O(4), located at the center of the vertical tunnel (in the center of each triangle formed by Ca(II) ions) [11]. The HAP in the hexagonal structure shows two channels along the c unit-cell axis deprived of PO_4 ions, which are filled by two Ca(I) ions at level z = 0 and z = 0.5. These calcium cations are nine-fold coordinated to the oxygen anions, O(3), of the phosphate anions, which allow the ion exchange of Ca^{2+}, H^+, and O^-. Two oxygen atoms of the PO_4 tetrahedra are located above and below mirror planes at heights of 0.25 and 0.75. The non-equivalent Ca^{2+} ions are located at two different positions: CaI at z = 0 and z = 1⁄2 along the three-fold axes ai (Wyckoff position 4f), and Ca(II) at z = 1⁄4 and z = 3⁄4 along the hexagonal screw axis parallel [00.1] (Wyckoff position 6h). Hence, considering the two non-equivalent

Ca positions, a more accurate formula of hydroxylapatite is $[(CaI)_4(CaII)_6]$ $(PO_4)_6(OH)_2$. The X anions are located at z = 1⁄4 and z = 3⁄4. Their exact positions depend on their size: the smaller F^- anion in fluorapatite is positioned exactly at the center of the triangles formed by the three CaII cations, the larger OH^- anion in hydroxylapatite is off-center by an increment δ = 0.36 Å [12]. The first two tunnels (tunnels I) are each filled by two calcium ions (at level z = 0 and z = 0.5), called Ca(1), which are nine-fold coordinated (D3h point group symmetry, 3+3+3) to the oxygen atoms of the phosphate groups called O(3). The six other calcium atoms form two triangles at levels z = 0.25 and 0.75, leading to a hexagonal-axis tunnel (tunnel II). These calcium atoms, called Ca(2), are seven-fold coordinated to six oxygen atoms of the phosphate groups O(3) and one oxygen of the hydroxyl groups, named O(4), located at the centre of the tunnel vertical axis, i.e. in the centre of each triangle formed by the calcium ions [13]. The geometric form of the unit cell is defined by three parallel hexagons with columnar Ca(I) on their corners, located at the two basal planes at z = 0 and z = 1, and at the equatorial mirror plane at z = ½. The hexagonal Ca(II) atoms are forming a pair of inner triangles at z = ¼ and z = ¾, and at $\pi/_3$ with respect to each other [14]. The six phosphate anions are distributed between two Ca^{2+} triangles in the interior of the unit cell. Three of the PO_4 tetrahedra are lying in Ca(II) triangles plane at z = 1/4, and three others are located at z = ¾. The calcium sites with different local environments are suggested to be the most favored for insertion of some metallic cations, such as Mg^{2+}. So, the HAP molecular unit cell is rearranged as $Ca(I)_4Ca(II)_6(PO_4)_6(X)$, characterized by a three-dimensional network of hexagonally packed PO_4^{3-} tetrahedral, and one hydroxyl anion. The OH^- is surrounding Ca^{2+} at the corners of the unit cell, whereas each of the PO_4^{3-} is shared by one column and delimits two types of channels. The columnar Ca(I) channel with a diameter of around 2.5 Å is surrounded by calcium cations coordinated with nine oxygen atoms and crosses the HAP matrix. Ca(I) atoms are occupying the six corners of the two basal planes and of the intermediate equatorial mirror plane, and each of the six calcium atoms is common with two adjacent cells. The screw-axis of the Ca(II) channel, having a diameter ranging from 3.0 to 4.5 Å, is surrounded by Ca^{2+} in coordination with seven oxygen atoms. The hexagonal Ca(II) is a contouring hexagon when projected on the basal plane. To balance the positive charge of the matrix, OH^- groups are hosted along the c-axis [15]. The OH^- groups are free to move along the Ca(II) channel which diameter is varying across the unit cell from about 2.85 Å in the center and on the basal plane (z = 0, z = ½), to around 2.73 Å at the two points between the basal planes and the center of the unit cell, lying in plane with the Ca(II) triangles (z = 1/4, z = 3/4). The inner hexagon-shaped overlapping these Ca(II) triangles(z = 1/4, z = 3/4) is located in the basal plane at π/3 with respect to each other. For this reason, the channel is considered a continuous ovoid cavity rather than a deep cylinder. The hydroxyl anions are arranged in an ordered column as OH^- OH^- …etc. The successive ordering and disordering effect is observed for OH^- lying in the channel, prolonged down the rotational symmetry axis of Ca(II) hexagons. The distortion of the phosphate network is, then, more required for the conservation of structural order in hydroxyapatite. The F and OH atoms exist in [001/4] and [00¾] anion columns at the edges of the unit cell. The anion column intersects each mirror plane in the center of an equilateral triangle of the three Ca(II) atoms. The adjacent calcium triangles at ½ unit cell above or below are rotated by π/3 around the screw axis. The F, Ca(II), P, and two O atoms are located in the mirror planes at (0,0, ¼) and (0,0, ¾). The six PO_4^{3-}tetrahedra inside the hexagonal unit cell are found between the pairs of Ca^{2+} in the outer hexagon. Three of these cations are lying on the Ca(II) triangle plane at z = 1/4, and the other three are on this triangle at z = ¾ [14]. Generally, the OH shows a disorder in the orientation

of the hexagonal form of HAP. One distinctive characteristic of this phosphate, in addition to inner channels, is the existence of proton exchange along the c-axis. Then, OH^- exchange is recognized to be faster than the exchange of surface calcium cations or phosphate anions. In addition to hexagonal and monoclinic structures, HAP exhibits an amorphous structure with no symmetry or long-range order. The interaction of OH, Ca, and PO_4^{3-} tetrahedra is governed by ionic interaction. The covalent interactions prevail between atoms within the phosphate anions and the O and H groups. Therefore, HAP is considered as repeating units of PO_4^{3-} tetrahedra linked by ionic interactions with Ca and OH groups [16]. In inorganic compounds, water often exhibits solid hydrates as isolated, channel, and metal-ion-associated sites [17-20]. No interaction is shown between water molecules in isolated hydrates, while in channel hydrates, H_2O molecules are interacting with each other, normally in one-dimensional channels or two-dimensional planes. In metal-ion associated hydrates, strong interactions of water are observed with transition or alkali metals. However, in apatite, H_2O is logging in several sites, including the ionic layer, hydroxyl, and calcium site vacancies. The adsorbed and inserted water molecules are located on the HAP surface, forming a "non-apatitic" hydrated ionic layer [21]. The surface area of apatite is then affected by diffusion rate, and as this surface increases, the rate of diffusion also increases, since there is more space for molecules to diffuse [22]. The theoretical investigations on dynamical processes at apatite surfaces show that an anisotropic diffusion inside particles is occurring within pore sizes ranging from 20-240 Å. Consequently, the surface porosity is governing the rate of diffusion, which is faster in the horizontal direction than in the orthogonal direction. Hydroxyapatite, whose pk_{ps} is around 59 at 25°C, is characterized by water insolubility, especially in alkaline medium. Due to the highly functionalized surface, this phosphate has excellent adsorption properties [23]. This sorbent is structured in two planes with different active sites, which are positively charged and consist of positively charged Ca-cations. One can note these sites are characterized by excellent sorbent properties toward acid molecules, whereas c-planes exhibit negatively charged phosphate and hydroxyl groups, supported with basic molecules [24]. The isoelectric point of the pure apatite (HAP) particles occurs at pH 6.5. Due to the presence of impurities, HAP exhibits diverse electrokinetic behaviors with isoelectric point (IEP) varying from 2.0 to 8.7. For dolomite ($CaMg(CO_3)_2$), the IEP is around 3.0-6.0 [25-27]. Apatite is a slightly soluble mineral, which can release the dissolved Ca^{2+} and Mg^{2+} to affect the surface electrical behaviors of minerals. The dissolved Ca^{2+} content in acid solutions is relatively high due to the carbonate and phosphate minerals reacting with hydrogen ions. But it decreases in an alkaline environment, which is due to the precipitation of $Ca(OH)_2$. The obtained point of zero charge (PZC) is around 3.3 for fluoroapatite. The quartz is the most electrostatically charged among the three ores. Generally, the dissolved Ca^{2+} and Mg^{2+} will affect the surface electrical behavior of minerals in solution [28]. This review will help researchers to document knowledge gaps and provide a reference for the efficient and green beneficiation of phosphate ores in the future.

2. Materials and Methods

2.1. Materials.

Dissimilar solutions of sodium hydroxide (NaOH) and nitric acid (HNO_3) were used for the potentiometric characterization of phosphate surface. Chemicals and reagents were of analytical grade from Sigma Aldrich and used without further purification. The stock 0.1M

solutions of NaOH and HNO_3 with 99.9% purity were diluted to employed solutions with concentrations of 0.05 M in 1000 mL of deionized water.

2.2. Methods.

The hydrated and activated Phosphate mineral samples were characterized by several techniques in order to examine the physical and chemical properties linked to the hydration behavior. Images, microstructure, and elemental spectra of the apatite samples were obtained from an energy dispersive X-ray spectrometer with a scanning electron microscope (EDX-SEM) (Jeol JSM-IT100 InTouchScope™) [16]. The surface characterization of apatite was performed by the batch equilibration technique applied to determine the Point of Zero Charge (PZC) and the Isoelectric Point (IEP). To achieve this purpose, monitoring the pH of suspension media of HNO_3 or NaOH (0.05 M)- phosphate systems was achieved at room temperature. Surface characterization against hydration and activation times was explored in 20-25 mL for HAP suspensions of 0.1 g/L.

3. Results and Discussion

One approximation of the PZC is the measurement of the IEP [30], which is determined by measuring the pH where the mineral particles do not move in an electric field (electrophoresis measurement) or coagulate in a suspension (flocculation measurement). If the PZC is determined by measuring the pH where the difference between H^+ and OH^- adsorbed on the mineral surface is zero, it is called the point of zero net proton charge (PZNPC). Adsorption of cations leads to a decrease in the PZNPC and to an increase in the IEP Table 1. Conversely, adsorption of anions leads to the opposite effect.

Table 1. The isoelectric point (IEP) is only representative of the external surface charges of particles in solution, whereas the point of zero charge (PZC) varies in response to the net total (external and internal) surface charge of the particles.

Temps	IEP or PZC
2h < 4h	4.9, 5.6, 7.2, 8.6,
<28h	4.7, 5.6, 7.2, 8.6, 9.9,
<48h	4.7, 6.4, 6.9, 7.4, 8.9, 9.9
6h, 4h	IEP: 6.3, 8.1, 8.9, 10.3.
28h	4.1, 4.5, 6.65, 9.3, 10.5.
56h	3.7, 4.9, 6.0, 8.2, 10.75
72h	IEP 4.0; PZC (6.4-7.3)
2.5-3h	IEP (8.1)
0-3h	IEP 8.85
72h	PZC 4.3, 4.4, 4.5 IEP 6.45-6.80
25-28h	(PZC) 8.6, 10.9
47-50h	IEP 3.55, 5.9, 7.4, 8.15-8.5, 9.95-10.0
6h, <4h	IEP 4.9, 5.4, 7.2, 8.6, 10, 11,
<28h	IEP 4.3-4.66, 5.7, 8.6, 9.9,
<58h	IEP 4.66, 6.4-6.9, 7.4, 8.9, 9.9

3.1. Variations of the atomic % Y=f(Ca), Y=Mg, Al, Si, P, F.

The atomic percentages of some metallic elements present in apatite are shown in the following figure. Phosphate mineral is hydrated for 24 hours and activated for durations varying between 10 min and 24 h Figure 1.

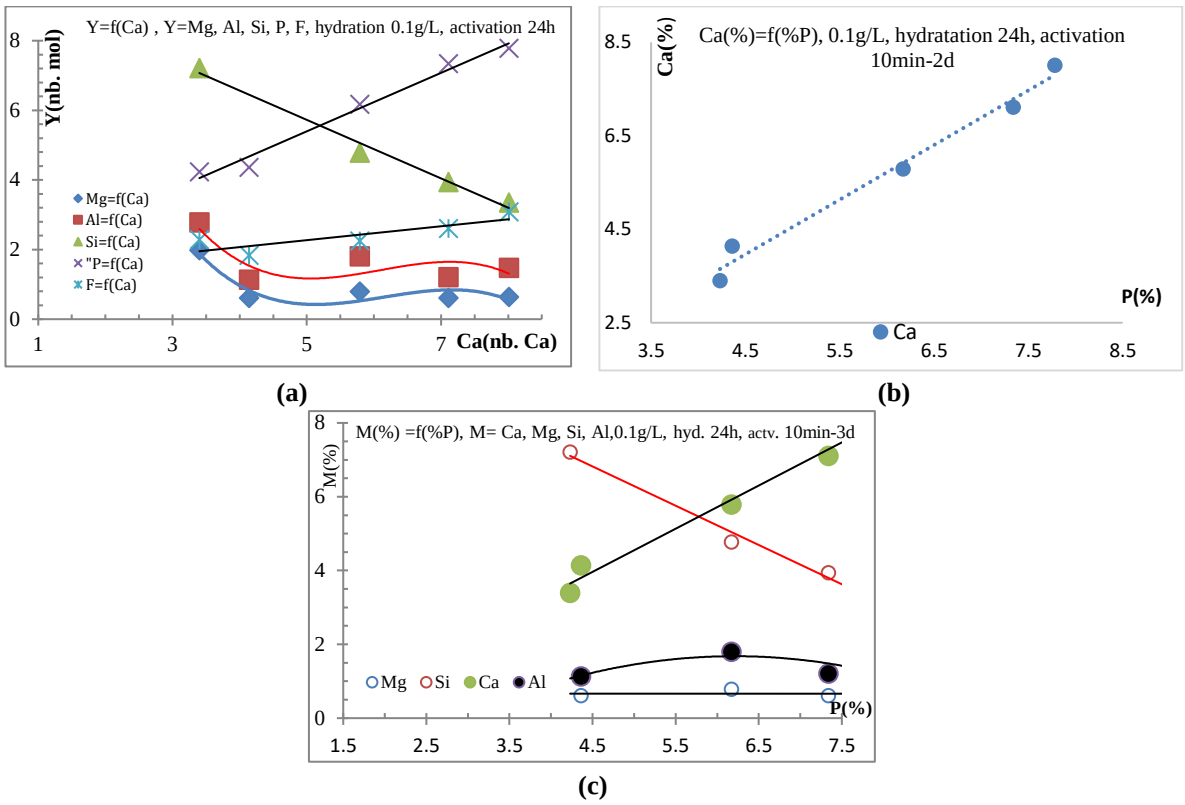

Figure 1. Variations of the atomic% Y=f(Ca), Y=Mg, Al, Si, P, F. m=0.1g/L, hydration 24 h, activation of 10 min to 3 days **(a)** Y=f(Ca), Y=Mg, Al, Si, P, F, hydration 0.1g/L, activation 24h; **(b)** Ca (%) =f(%P), 0.1g/L, hydration 24h, activation 10min-2 days; **(c)** M (%) =f(%P), M= Ca, Mg, Si, Al, 0.1g/L, hydration 24h, activation 10min-3 days.

Surface properties of apatite are governed by its composition, characterized by the calcium ratio to different impurities including Mg, Al, Si, P, and F. Phosphate mineral dispersion is characterized by a deficiency in calcium, characterized by a Ca/P atomic ratio of 1.17, which is lower than that of stoichiometric (1.67) HAP.

$$Ca\ (\%) = f(\%P) = 1.17x - 1.30, R^2 = 0.98 \quad (1)$$

$$Si\ (\%) = f(\%P) = -1.10x + 11.61, R^2 = 0.99$$

$$P = f(Ca) = 1.17x - 1.30, R^2 = 0.98$$

$$P = f(Ca) = 0.84x + 1.20, R^2 = 0.98$$

$$Si = f(Ca) = -0.84x + 9.93, R^2 = 0.99$$

$$F = f(Ca) = 0.20x + 1.27, R^2 = 0.69$$

3.2. Morphology of phosphate mineral – energy dispersive X-ray spectrometer (EDS).

The morphology of the apatite powder particles hydrated for 2,24,72 hours and activated at 10 min to 3.5 h is observed using a scanning electron microscope (Figure 2) attached with an energy dispersive X-ray spectrometer (EDS) (Table 2 – Table 3).

The morphology of the phosphate mineral observed in the image reveals a granular structure with individual particles and a rough surface, indicating aggregates of crystals or nonhomogeneous grains. The particle sizes, on the order of a few micrometers, show a size distribution that could influence the physicochemical properties of the phosphate. The numbers present in the image indicate points of interest, suggesting a targeted analysis of specific areas within the sample (Tables 2, 3, and Figure 3).

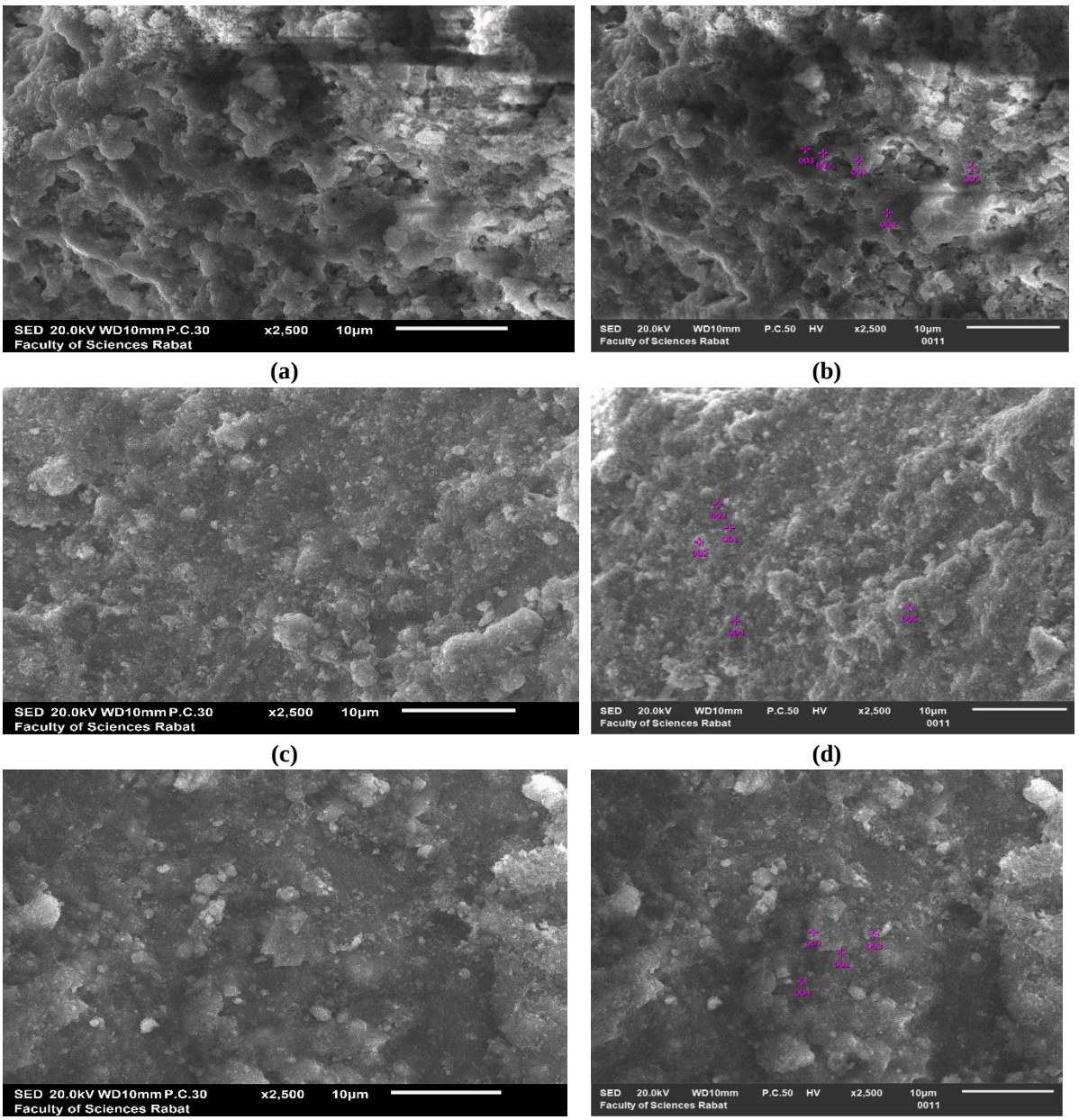

Figure 2. The morphology of the apatite m=0.1g/L powder particles hydrated for **(a,b)** hydration 2 hours; **(c,d)** hydration 24 hours, activation of 10 min to 3 days; **(e,f)** hydration 72 hours.

Table 2. m=0.1g/L, 2 hours of hydration.

Formula	eds1	eds2	eds3	eds4	eds3
O	57.04	45.16	42.71	39.04	34.18
F	2.71	0.69	0.77	2,40	0.59
Mg	0.39	0.55	0.27	-	-
Al*	0.43	0.95	0.40	0.18	-
Si	1.86	2.46	0.57	0.88	0.48
P	16.02	20.02	15,16	19.87	24.35
Ca	21.38	26.98	37,38	37.63	37.62
Fe*	0. 17	-	-	-	-

Table 3. m=0.1g/L, 24 hours of hydration.

Formula	Atom%	Eds4(13)	Eds1(23)	Eds2(14)	Eds3
O	57.4(1)	74.51(2)	76.93(5)	77.31(4)	74.65(3)
F	1.83	2.60	2.28	2.25	3.08
Mg*	0.61	0.61	1.98	0.79	0.64
Al*	1.13	1.21	2.78	1.80	1.47
Si	2.76	3.94	7.21	4.78	3.35
P	4.36	7.34	4.23	6.17	7.78

Formula	Atom%	Eds4(13)	Eds1(23)	Eds2(14)	Eds3
Ca	4.14	7.11	3.40	5.79	8.01
Ti	0.23	0 1	0	0	0
Fe*	0.21	0.21	0	0	0

Energy Dispersive Spectroscopy (EDS) is a technique used to determine the elemental composition of materials. It operates by detecting X-rays emitted from a sample when excited by an electron beam in a scanning electron microscope (SEM) (Figure 3).

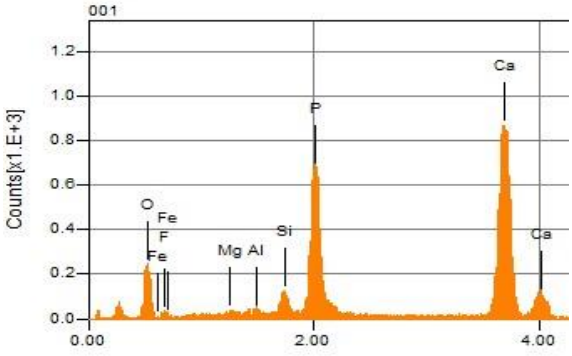

(a)

Formula	Atom%
O	57.04
F	2.71
Mg*	0.39
Al*	0.43
Si	1.86
P	16.02
Ca	21.38
Fe*	0.17
Total	100.00

(b)

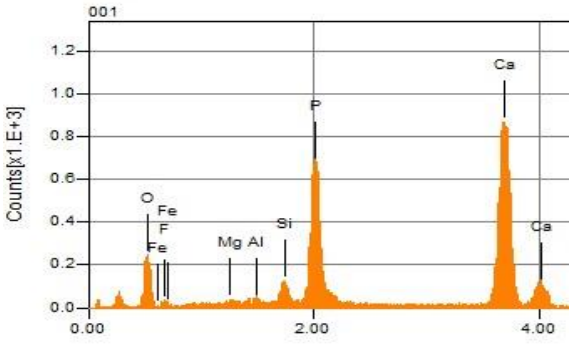

(c)

Formula	Atom%
O	74.51
F	2.60
Mg*	0.61
Al*	1.21
Si	3.94
P	7.34
Ca	7.11
Fe*	0.21
Total	100.00

(d)

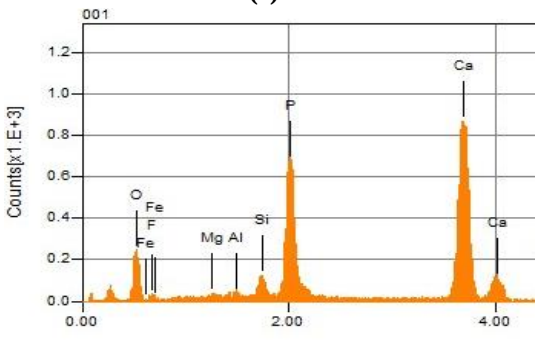

(e)

Formula	Atom%
O	66.85
F	0.91
Mg*	0.57
Al*	0.74
Si	25.76
P	1.86
Ca	2.94
Fe*	0.21
Total	100.00

(f)

Figure 3. EDS spectrum of the apatite powder, hydration 2h, activation 0-3.5h. **(a,b)** Hydration 2 h; **(c,d)** Hydration 24 h; **(e,f)** Hydration 72 h.

The EDS analysis (Figure 3) shows the presence of the four main peaks corresponding to Ca, P, O, and Si. The phosphate-hosted impurities correspond to magnesium, aluminum, and iron metals. The Ca/P ratio is examined in relation to the time of hydration as an important parameter for the charge equilibrium in the range of 0 to 51 hours.

3.3. Variations of $\Delta pH=f(pH_f)$.

The intersection points of ΔpH=f (pH) curves are the IEP. As found, IEPs are constant and do not depend on time, suggesting, therefore, a physisorption phenomenon in external

surfaces. There is a point of zero charge where ΔpH=0, and this point differs from the IEP if any specific adsorption of electrolyte ions occurs. As shown, the factor (PZC-IEP) is not zero when equilibrium is not reached. The IEPs found are correlated to several processes of surface protonation and charge development at the apatite-water interface [31].

Figures 4-9 show the curves of ΔpH vs. final pH obtained using the fit method of pH=f(t). As shown, the phosphate surface exhibits strong pH dependence.

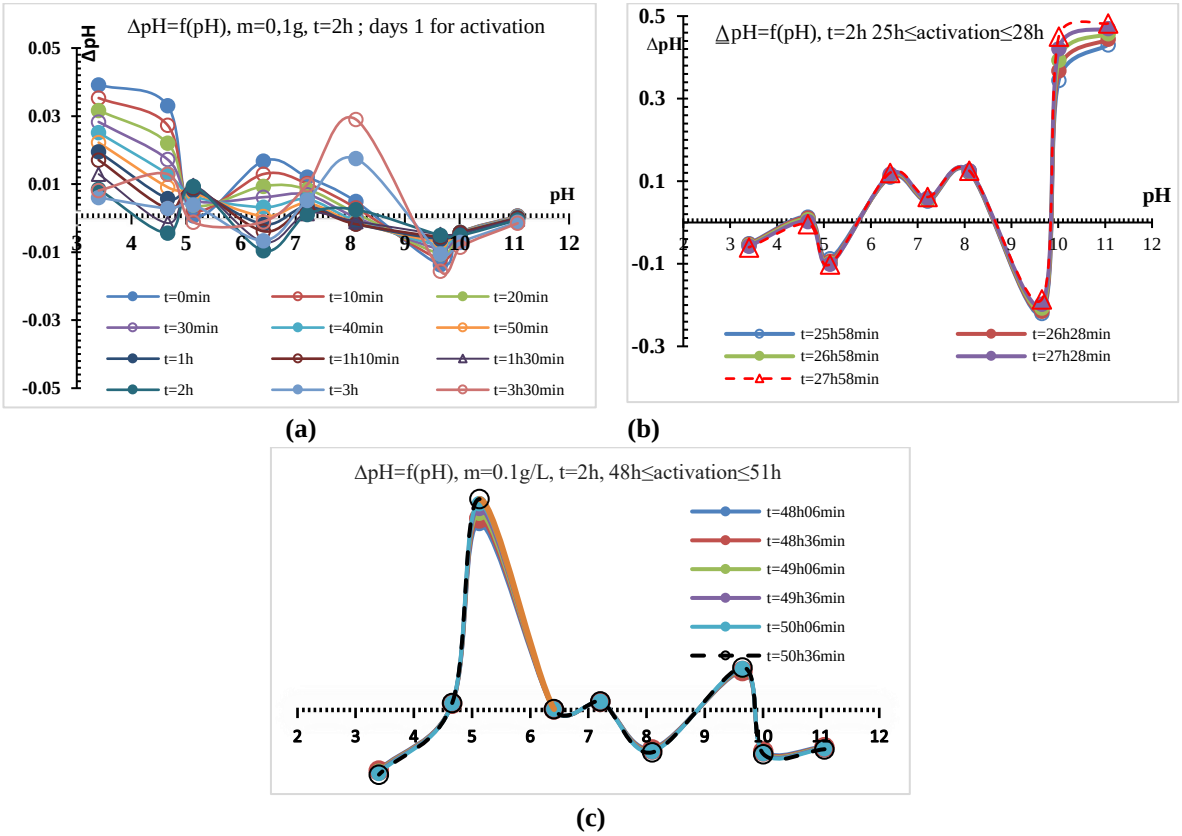

Figure 4. Variations of ΔpH=f(pH) obtained at hydration of 2 h, for natural apatite at m=0.1g/L, and activation time of 0 to 50.5h.**(a)** ΔpH=f(pH), m=0.1g/L, t=2h; days 1 for activation; **(b)** ΔpH=f(pH), t=2h 25h≤activation≤28h; **(c)** ΔpH=f(pH), m=0.1 g/L, t=2h, 48h≤activation≤51h.

The phosphate mineral doesn't have a single defined isoelectric point, making it difficult to infer these points to various oxides present in the phosphate matrix. Figures 4-9 indicate that activation of 1 to 2 days leads to similar values of IEP and PZC. In contrast, slight activation, less than 4 h, results in a significant shift in PZC that decreases as activation duration increases. Accordingly, the lack of correspondence between the isoelectric point and point of zero charge of the solid suggests that different equilibria govern the sorption. The change in point of zero charge is due to the kinetic alteration of surface phosphate material. Thus, chemisorption of electrolyte ions is the main factor associated with the protonation equilibrium of the surface sorbent. Hence, the similarity of PZC and IEP is valid only if there is no adsorption of ions other than H^+ and OH^- occurring. The following values of IEP of 4.9, 5.6, 7.2, and 8.6 are obtained for activation of about 4h, 4.7, 5.6, 7.2, 8.6, and 9.9 for 22h, and 4.7, 6.4, 6.9, 7.4, 8.9, and 9.9 for 40h. As found, the lower value of PZC compared to that of IEP indicates the specific adsorption of anion electrolyte [24]. At hydration of 3.5 h, there are various crossing points of ΔpH=f(pH) occurring in the range 5.7-6.0. Specific adsorption of the background electrolyte (Na^+, Cl^-) is occurring in these conditions [23].

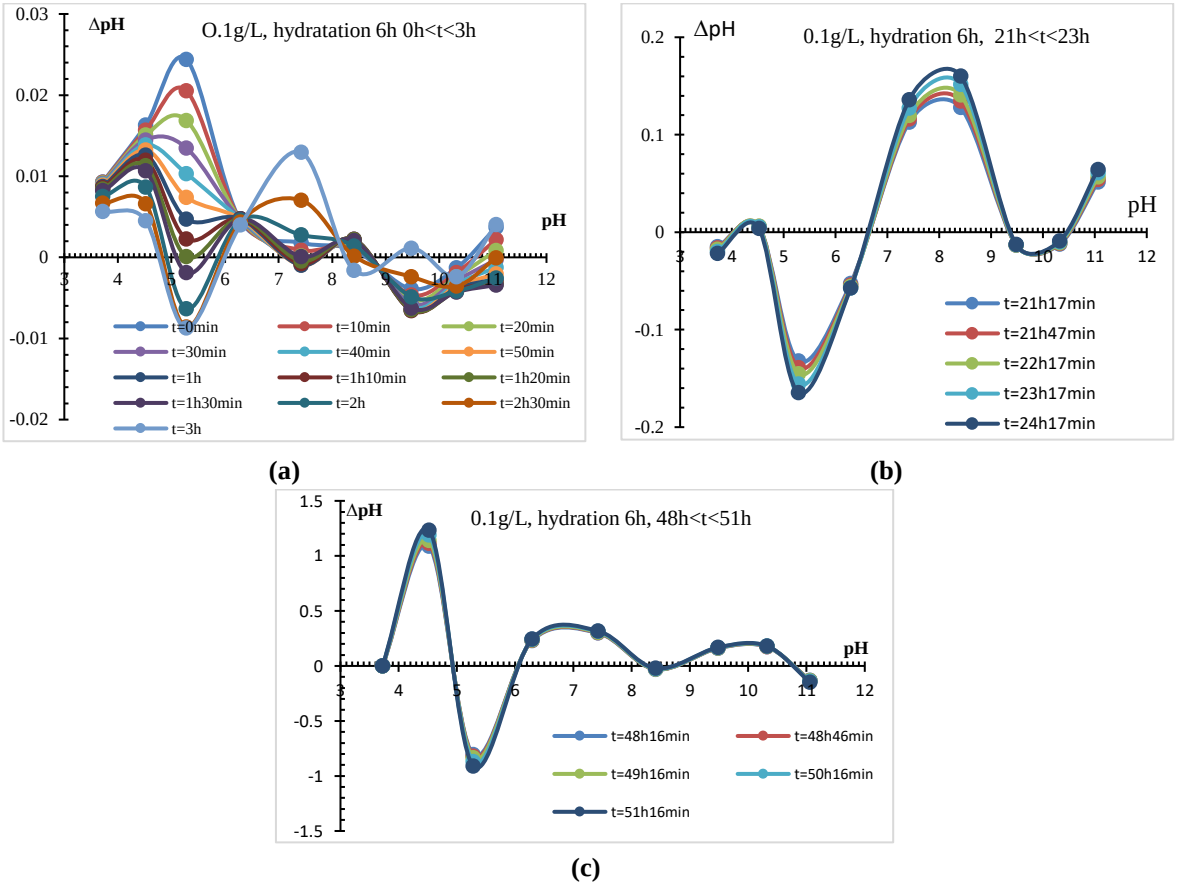

Figure 5. Variations of ΔpH=f(pH$_f$) obtained at hydration of 6 h, for natural apatite at m=0.1g/L, and activation time of 0 to 50.5h. **(a)** O.1g/L, hydration 6h 0h<t<3h; **(b)** 0.1g/L, hydration 6h, 21h<t<23h; **(c)** 0.1g/L, hydration 6h, 48h<t<51h.

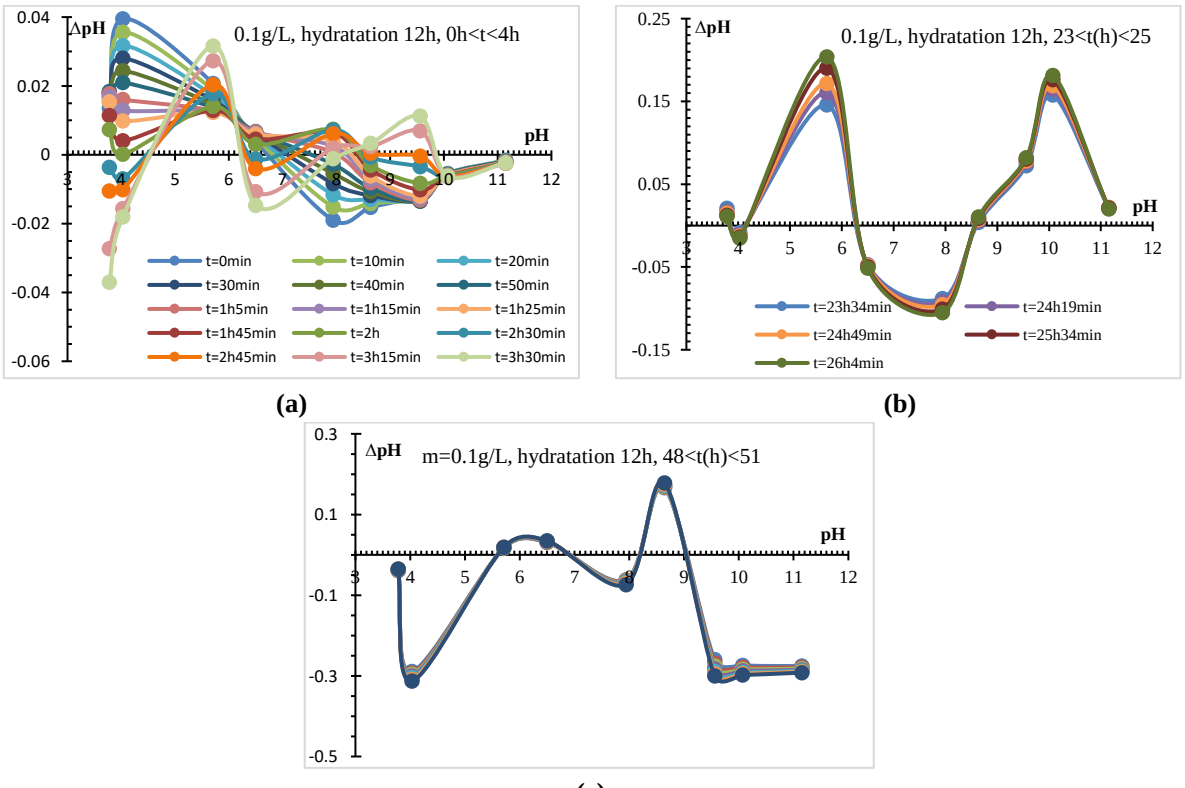

Figure 6. Variations of ΔpH=f(pH$_f$) obtained at hydration of 12 h, for natural apatite at m=0.1g/L, and activation time of 0 to 50.5h. **(a)** 0.1g/L,hydratation 12h, 0h<t<4h; **(b)** 0.1g/L, hydratation 12h, 23<t(h)<25; **(c)** m=0.1 g/L, hydratation 12h, 48<t(h)<51.

It is assumed that near the PZC, three types of active sites are contributing to ion adsorption: $-OH_2^+$, -OH, and $-O^-$. For synthetic phosphates, a high PZC (>7.0) is generally associated with the prevailing of (> $\overline{CaOH}$ sites, whereas decreasing PZC values reveal a predominance of (>POH) sites [17]. The mass titration and isoelectric point techniques are used to estimate the PZC of simple oxides. For this purpose, the point of zero charge must be fairly constant. Extensive shifts reported in PZC are assumed to be owing to the nature of the used electrolyte, solid-to-liquid ratio, and aging [18].

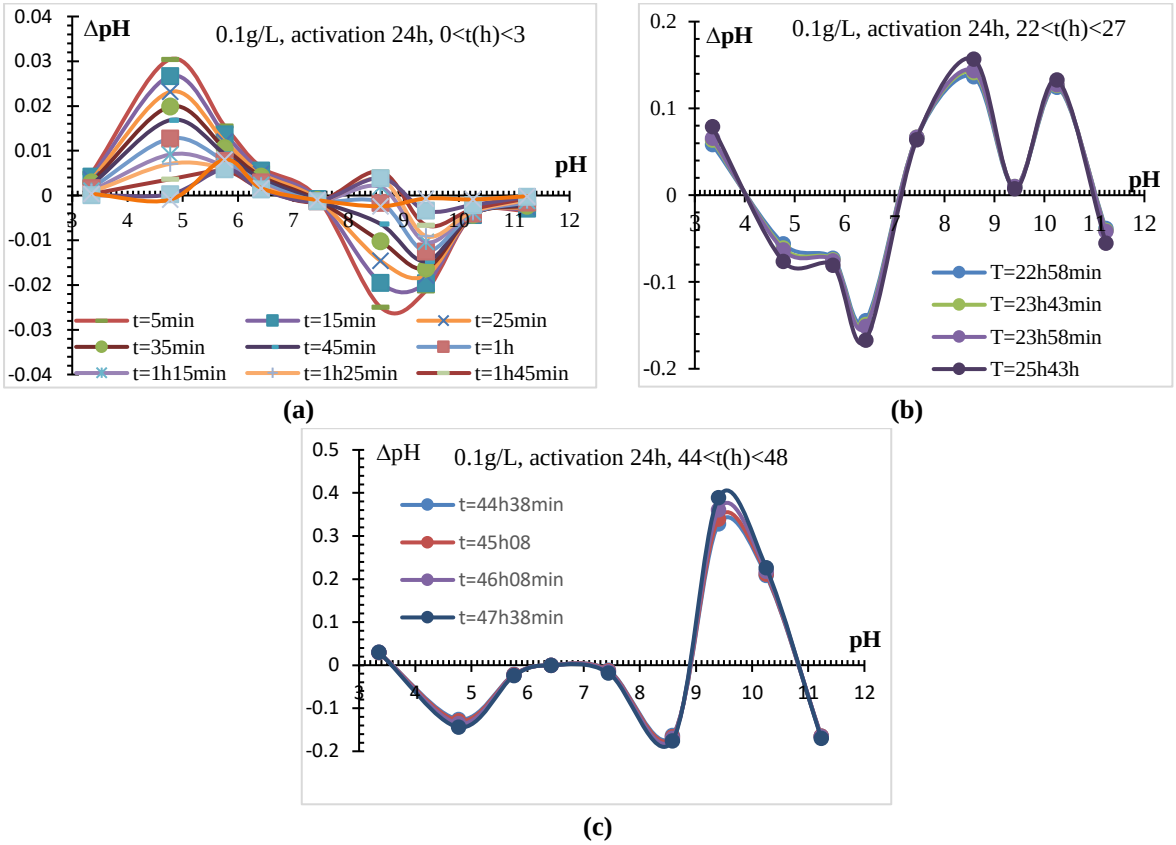

Figure 7. Variations of $\Delta pH=f(pH_f)$ obtained at hydration of 24h, for natural apatite at m=0.1g/L, and activation time of 0 to 50.5h.**(a)** 0.1g/L, activation 24h, 0<t(h)<3; **(b)** 0.1g/L, activation 24h, 22<t(h)<27; **(c)** 0.1g/L, activation 24h, 44<t(h)<48.

It is then suggested that the differences in the PZC and IEP are not fully understood, and more investigations are required for this purpose. Hence, the outstanding results are suggested to be due to material impurities rather than to the sorbent surface properties. Irregular isoelectric point for the same solid is usually attributed to the hydration and crystallographic structure. As observed, H^+/OH^- physisorption is accomplished at the pH of the isoelectric point, while chemisorption is occurring at the point of zero charge. Consequently, PZC values are a function of hydration time [32-34]. The discrepancies between IEP and PZC values are a function of the specific adsorption of the electrolyte salt ions (Na+, Cl^-) onto the apatite surface. At short hydration time less than 4h, the downward shift in the PZC is due to specific adsorption of Na^+ onto the apatite surface, whereas the specific adsorption of NO_3^- or Cl^- shifts PZC towards higher values. From the literature, the IEP is observed to shift in the opposite direction of PZC [35]. As found, the specific adsorption of electrolyte cation in a Stern-type layer makes the H^+ adsorption more difficult, leads to the release of protons ($\Delta pH<0$), and shifts the PZC to lower values. Similar adsorption of anion is associated with proton uptake that results in $\Delta pH>0$ and a higher PZC.

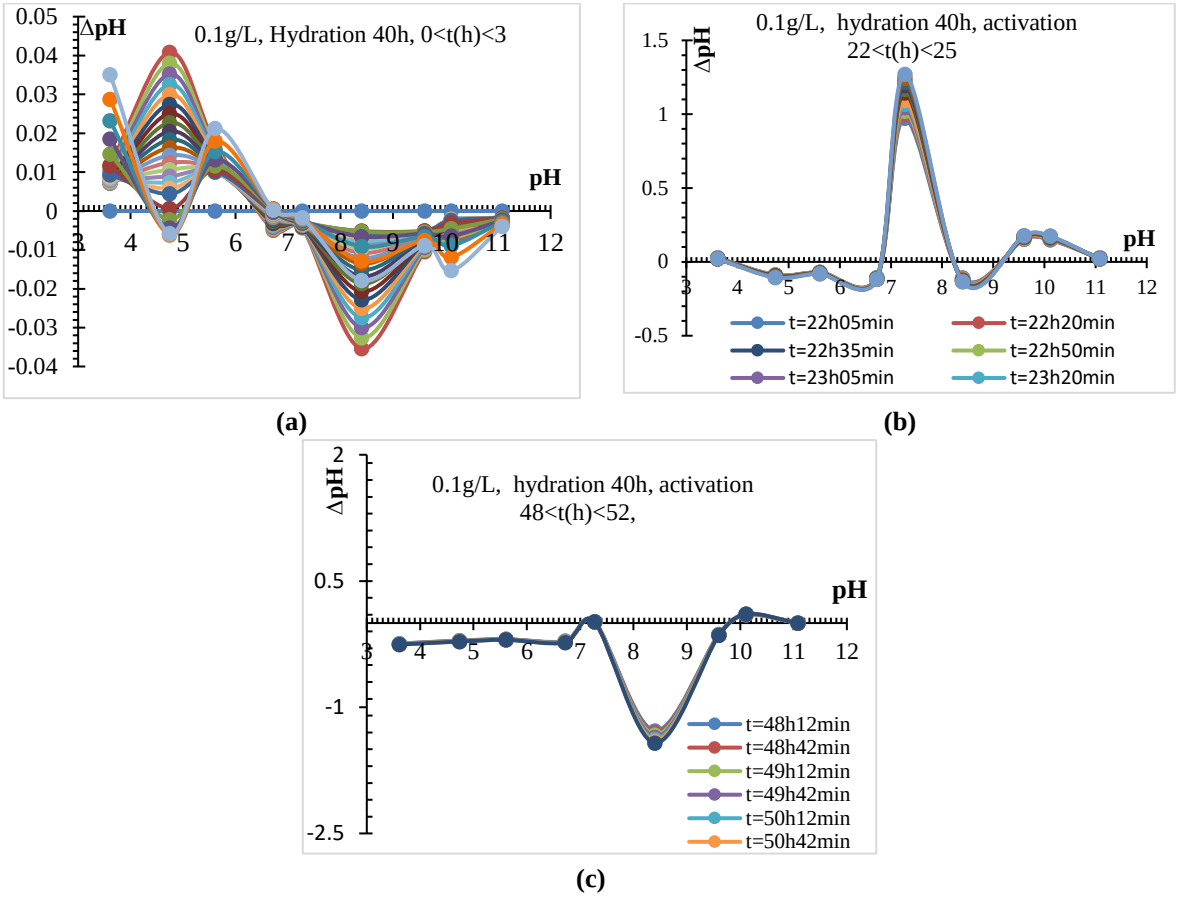

Figure 8. Variations of ΔpH=f(pH$_f$) obtained at hydration of 40 h, for natural apatite at m=0.1g/L, and activation time of 0 to 50.5h.**(a)** 0.1g/L, Hydration 40h, 0<t(h)<3; **(b)** 0.1g/L, hydration 40h, activation 22<t(h)<25; **(c)** 0.1g/L, hydration 40h, activation 48<t(h)<52.

The change in PZC stipulates that the amounts of H^+ and OH^- exchanged with the surface site are not equal. It is important to note that the isoelectric point, which characterizes the external surface charges of phosphate mineral particles in solution, remains unchanged with activation time. This is a result of physisorption at the external surface. The point of zero charge fluctuates in response to the variation of the internal surface charge of the particle suspensions. The difference (PZC - IEP) symbolizes the measure of surface charge distribution of porous phosphate. Values higher than zero correspond to more negatively charged external than internal particle surfaces, while values near zero characterize a more homogeneous distribution of the surface charges [36]. The IEP of these minerals can range from ~2 for amorphous SiO_2 to 9.3 for γ-Al_2O_3 and 11.6 for MgO [37]. Activation of phosphate suspension for a duration lower than 4 hours results in IEPs that are equal to 4.9.0, 5.6, and 8.6. Equal values of PZC and IEP are obtained during ΔpH experiments undertaken for 24 and 48 h on activated samples. The physisorption is then prevailing in these conditions. Asymptotic behavior is observed for activation at 25 h at pH around 9.9. As shown, the PZC value lies in these conditions within the range 6.0-7.1, for a minimal activation duration of about 1h. At equilibration ranging from 2 to 3.5h, PZC and IEP move to 9.2. From the EDS results, the shift and disappearance in isoelectric points of 4.9 and 5.6 for hydration higher than 3.5 h is due to the total solubility of ferric oxyhydroxides present in apatite, for which IEP is prevailing at pH 6.4. The disappearance of the EDS peak of this hydroxide occurring at activation higher than 4 hours supports the total dissolution of hematite and goethite, whose IEPs are 4.9 and 5.6. The IEP/PZC of rutile under the same conditions is also located at pH 5.6 [38-42]. Accordingly, a similar IEP (PZC) value of 6.3 ± 0.2 is obtained at different ionic strengths, for the synthetic

apatite and fluoroapatite from titration curves, potentiometric mass, time, and surface charge titration techniques [24,43]. The dispersion interaction between the apatite and interface molecules forming is a short-distance interfacial structure [14,44]. The value difference observed between IEP and PZC suggests that electrolyte ions are exchanged between the apatite surface and the first water layer [45]. The dispersion interaction of the sorbent with interface molecules forms a short-distance interfacial structure. As a result, the experimental shift in PZC observed at a short hydration is controlled by a surface dipole moment of this structure induced by the charge redistributions of adsorbed water molecules. During hydration, strong columbic interactions of water are occurring with the calcium and the phosphate ions of the apatite surface. These interactions are found to prohibit hydrogen bonds of interfacial water with the hydroxide ions [46-48].

Generally, phosphate rocks are associated with gangue minerals that affect surface chemistry. As obtained, this gangue consists of the silicate in addition to iron, magnesium, and aluminum oxides [6,49,50]. Consequently, the surface charge of this mineral depends on the extent of these oxide impurities, which are the main constituents of apatite. The aluminosilicate contains hydrated exchangeable cations, primarily Ca^{2+} and Mg^{2+}, in the interlayer. The reported isoelectric points of calcite and apatite are about 10.5 and 7.4, respectively. In the presence of apatite as supernatant, the IEP of calcite is reduced from 10.5 to 6.5 [51]. The pH value of the isoelectric point of Fe_2O_3 is found to be 7.2, which is shown to shift to 9.2 at activation of 3.0 and 3.5 h. This oxide is totally dissociated after 24 h. The IEP values of the aluminosilicate (Al_2SiO_5) and magnesium silicate ($MgSi_2$) mixtures are found to increase from 1.4 for silica to 7.1 and 10.1 for pure alumina and magnesia, respectively [52,53]. The IEP of the apatite minerals is reported at variant pH of 3.5, 4.2, 5.5, 6.7, and 7.5 [54]. The IEP values of apatite are related to the ratio(R) of Fe, Mg, and Al to SiO, which varies due to dissolution effects. The shift of this ratio results in a move of surface properties that influence the isoelectric point. The higher this ratio, the higher the isoelectric point. Taking into account these results, the IEPs of 4.9, 4.7, and 5.6 must be associated with Hematite (Fe_2O_3), silico-aluminophosphate or Kaolinite (Al_2O_3 $2SiO_2$•$2H_2O$), hydrated molybdenium silicate, and calcium phosphates. According to previous studies, the IEP of 7.2, not observed for 40 h of hydration, is attributed to hematite (Fe_2O_3)/SiO_2 (1%). The surface charge of aluminosilicates depends on the amount of SiO_2, MgO, Al_2O_3, and Fe_2O_3 in the sample, which are the main constituents of natural phosphates. The average isoelectric point of this silicate is observed in the range between 9.4 and 9.8 [55-57]. The IEP observed at pH 6.9 and 9.8 are previously attributed to the outer bottom and pore wall of alumina, respectively. As discussed, the surface of aluminum oxide appears more like Al $(OH)_3$ or Al_2-OH, than Al_2O_3, with IEPs of 8.9 and 9.9, respectively, in Table 4. The formation and co-occurrence of gibbsite ($AI(OH)_3$), boehmite (AIOOH), and alumina (Al_2O_3) are concomitant [58]. Reported values for the isoelectric points of magnesium oxide, not observed at hydration of 3.5 to 50 hours, range from 10.5 to 12.5. For pH lower than 10.5, the surface is positively charged in the form of $MgO–OH_2^+$ [59-61]. The surface hydroxyl groups involved in this exchange result from the activation process carried out in the dissociation of chemisorbed water.

Table 4. IEPs and PZCs at hydration of 72 h.

IEP at hydration of 72 h	PZC at hydration of 72 h
IEP 4.0 (1.5-3h), (8.1 (0-2h)), 8.85(0-3h)	PZC 6.4-7.3 (2.5-3h)
IEP 4.3, 4.4, 4.5, 8.6, 10.9 (25-28h)	PZC 6.45-6.80 (25-28h)
IEP 3.55, 5.9, 7.4, 8.15-8.5, 9.95-10.0 (47-50h)	-

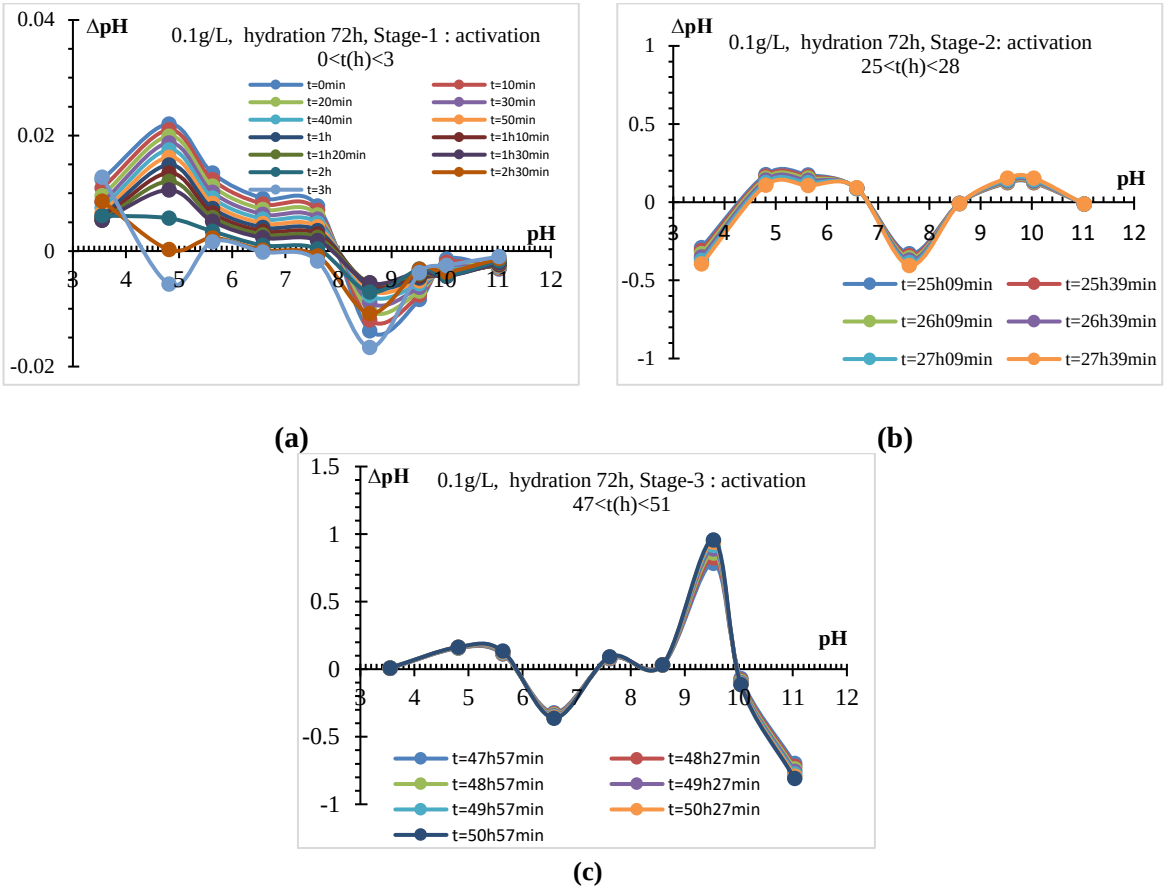

Figure 9. Variations of $\Delta pH=f(pH_f)$ obtained at hydration of 72 h, for natural apatite at m=0.1g/L, and activation time of 0 to 50.5h, **(a)** Stage-1: activation 0<t(h)<3; **(b)** Stage-2: activation 25<t(h)<28; **(c)** Stage-3: activation 47<t(h)<51.

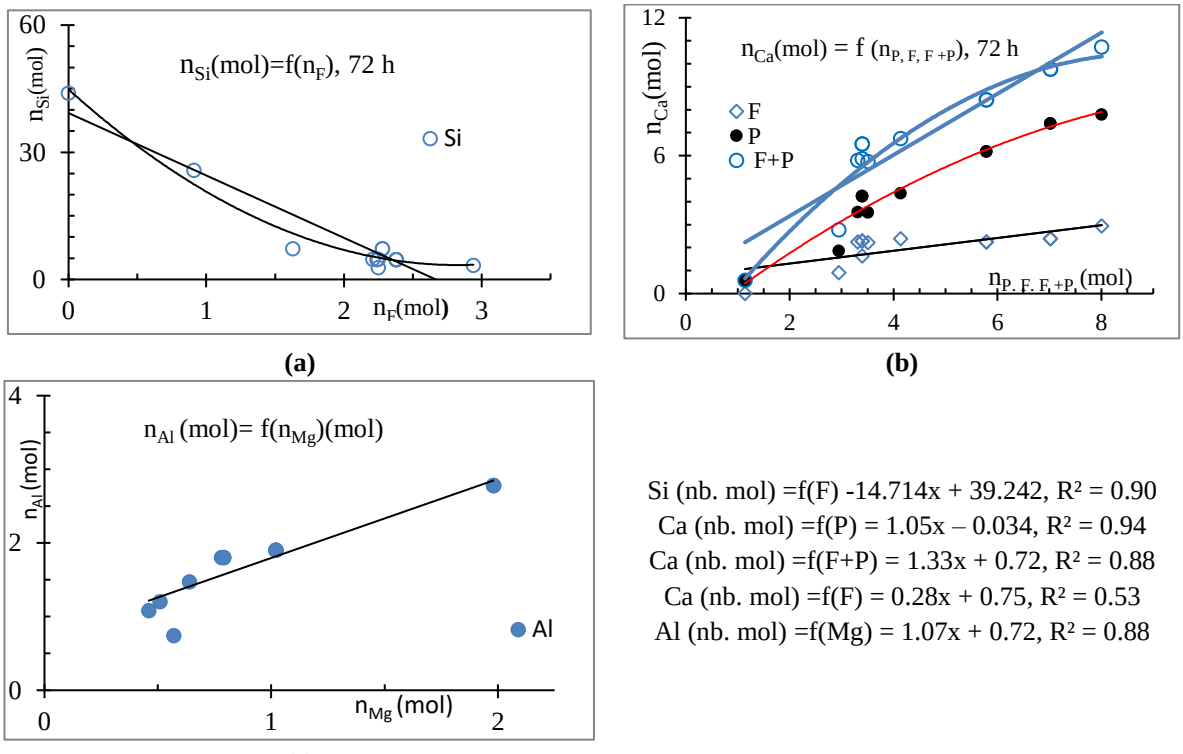

Si (nb. mol) =f(F) -14.714x + 39.242, R^2 = 0.90
Ca (nb. mol) =f(P) = 1.05x – 0.034, R^2 = 0.94
Ca (nb. mol) =f(F+P) = 1.33x + 0.72, R^2 = 0.88
Ca (nb. mol) =f(F) = 0.28x + 0.75, R^2 = 0.53
Al (nb. mol) =f(Mg) = 1.07x + 0.72, R^2 = 0.88

Figure 10. Variations $n_{Si}(mol)=f(n_F)$, $n_{Ca}(mol) = f (n_{P, F, F +P})$, and $n_{Al} (mol)= f(n_{Mg})(mol)$ obtained at hydration of 72 h, for natural apatite at m=0.1g/L.Table 4. **(a)** $n_{Si}(mol)=f(n_F)$, 72 h; **(b)** $n_{Ca}(mol) = f (n_{P, F, F +P})$, 72 h; **(c)** $n_{Al} (mol)= f(n_{Mg})(mol)$.

From these results, the variation in the PZC values obtained at low activation time and the specifically adsorbed ions are due to the failure to achieve equilibrium activation in terms of mineral protonation/deprotonation. At higher activation, calcium and phosphate ions resulting from apatite dissolution are co-adsorbed on alumina and strongly affect the surface potential, whereas hematite (Fe_2O_3) is dissolved in these conditions [62]. It is shown previously that the shift in IEP with the time of equilibration is attributed to the zeta-potential measuring [63]. From these results, Figures 9 and 10 show that the hydration time of 72 hours and activation of 4 hours are insufficient to reach solubility equilibrium. Dissimilarity in PZC and IEP values is correlated with the stability of hydroxyapatite. The change of PZC associated with a defined IEP is governed by the acid-base properties of various $\overline{>SOH}$ groups. Apatite rock dissolution rises continually, and the PZC fluctuates until an equilibrium state is reached at activation of 24 hours. The difference in apatite surface properties is most associated with the activation rather than the hydration process. As shown in Fig. 9, the deprotonation pH(ΔpH<0), which initially varies from 8.0 to 9.5, moves slowly from 6.8 to 8.6 and 7.6, within activation times (t_{ac}) of about 26 and 49 h, respectively. Also, important alkaline behavior is observed at high `` $t_{ac}$`` for pH ranging from 8.6 to 10.0, with a maximum at pH 9.5.

A buffering effect is occurring at low activation in the pH range of 5.6-7.0, which corresponds to (pK_a-1, pK_a+1) =6.6. Based on the obtained data, values of surface ionization of Fe_2O_3-SiO_2 obtained at `` $t_{ac}$`` ranging from 1.5 to 3.5h are $pK_a(\overline{>FeOH_2^+}, \overline{>FeOH})$=6.6. The isoelectric points of 3.5 and 4.5 obtained at ``$t_{ac}$`` higher than 24 h are linked to Kaolinite ($Al_2O_3 \cdot 2SiO_2 \cdot 2H_2O$), which, under similar conditions, reveals various behaviors, due to the Al/Si ratio(R) variation, which defines the surface properties. At activation durations ranging from 25 to 50 h, a significant difference in the IEP values is observed for the Al_2O_3-SiO_2 composite. At low ``R`` values, this oxide surface is covered with a SiO_2 layer with isoelectric points of 4.0, 4.4, and 4.6. Also, the IEP of serpentine ($Mg_3Si_2O_5(OH)_4$) is found to be 4.0 [63,64]. As found previously, the IEP of the apatite at `` $t_{ac}$`` around 25 h is found to be about 6.4-6.8. The higher IEP=PZC value of 6.8 results from the slight protonation of the external surface occurring for pH ranging from 4.8 to 6.7. Previous results show that the synthesized hydroxyapatite has a point of zero charge of 6.5 and an isoelectric point less than 5, due to adsorption reaction. Such a mild surface acidity effect is responsible for the scatter in the point of zero charge [63]. For PZC greater than IEP, this adsorption is associated with positively charged surfaces [24]. As can be seen from ζ-potential measurements of HAP, IEP is increasing from pH 6 to about pH 8, when the aging time is increasing from 10 min to 7 days. An isoelectric point ranging approximately from 6.0 to 6.4 is achieved for 2 days. Owing to the hydration phenomenon, protonation/deprotonation is suggested to influence the particle charge [14]. It is also proposed that the increase in IEP PZC values must be attributed to the interaction of electrolyte cation (K^+) with mineral surface [64].

4. Conclusions

Phosphate ore is the dominating natural resource for the production of fertilizers and phosphorus chemical products. Because of the presence of several ions in its formula, apatite is a very suitable host for various substituents. Moreover, apatite finds many applications in various areas, and its biological properties are not the least important ones. Properties of apatite depend on its composition, including the Ca/P ratio. Phosphate mineral dispersion is characterized by a deficiency in calcium, characterized by a Ca/P atomic ratio of 1.17, which

is lower than that of stoichiometric (1.67) HAP. The zero charges (PZC) and isoelectric point (IEP) of phosphate were determined by the derivative potentiometric titration technique. The discrepancy between PZC and IEP is then important for the characterization of the chemical nature of the activation process. The phosphate mineral doesn't have a single defined isoelectric point, making it difficult to infer these points to various oxides present in the phosphate matrix. The change in point of zero charge is due to the kinetic alteration of surface phosphate material. The mass titration and isoelectric point techniques are used to estimate the PZC of simple oxides. The outer surfaces of apatite are rapidly protonated/deprotonated and remain unchanged due to the physisorption, while the internal surface results in a variable PZC at low activation time.

Author Contributions

Conceptualization, M.K., F.E.M., and H.K.; methodology, M.K. and F.E.M.; software, A.B. and F.E.M.; validation, M.K., F.E.M., and H.K.; formal analysis, F.E.M.; investigation, F.E.M. and M.K.; resources, A.B. and S.B.; data curation, H.K. and M.K.; writing—original draft preparation, F.E.M.; writing—review and editing, S.B. and M.H.; visualization, M.K. and M.H.; supervision, A.B. and S.B.; project administration, A.B. and S.B.; funding acquisition, not applicable. All authors have read and agreed to the published version of the manuscript. All authors must confirm their agreement with the contribution statement before submission.

Institutional Review Board Statement

Not applicable.

Informed Consent Statement

Not applicable.

Data Availability Statement

The data of this study are available from the corresponding author upon reasonable request.

Funding

This research received no external funding

Acknowledgments

All authors would like to thank the staff of the Laboratory of Chemistry of Materials and Environment, Faculty of Sciences, Mohammed V University in Rabat, Morocco, for their technical support and assistance during the experimental work. We also acknowledge the use of laboratory equipment provided by the institution.

Conflicts of Interest

The authors declare no conflict of interest.

References

1. Ruan, Y.; Zhang, Z.; Luo, H.; Xiao, C.; Zhou, F.; Chi, R. Effects of Metal Ions on the Flotation of Apatite, Dolomite and Quartz. *Minerals* **2018**, *8*, 141, https://doi.org/10.3390/min8040141.
2. Swain, S.; Patra, A.; Dwibedy, P.; Guru, B.M.P.; Rautray, T.R. 5 - Electrochemical synthesis of ceramics for biomedical applications. In Advanced Ceramic Coatings for Biomedical Applications, Gupta, R.K., Motallebzadeh, A., Kakooei, S., Nguyen, T.A., Behera, A., Eds.; Elsevier: **2023**; pp. 87-110, https://doi.org/10.1016/B978-0-323-99626-6.00007-X.
3. Zhang, X.; Tao, Y.; Ma, F. Application of Falcon centrifuge in the separation of siliceous phosphate ore. *Particulate Science and Technology* **2022**, *40*, 958-971, https://doi.org/10.1080/02726351.2022.2027056.
4. Berzin, S.V.; Konopelko, D.L.; Petrov, S.V.; Proskurnin, V.F.; Berzon, E.I.; Kurapov, M.Y.; Golovina, T.A.; Chernenko, N.Y.; Chervyakovskiy, V.S.; Palamarchuk, R.S.; Andreeva, E.M. Evaluation of Granite Fertility Utilizing Porphyry Indicator Minerals (Zircon, Apatite, and Titanite) and Geochemical Data: A Case Study from an Emerging Metallogenic Province in the Taimyr Peninsula, Siberian High Arctic. *Minerals* **2024**, *14*, 1065, https://doi.org/10.3390/min14111065.
5. Das, S.; Swain, S.; Rautray, T.R. Incorporation of hydroxyapatite and cerium oxide nanoparticle scaffold as an antibacterial filler matrix for biomedical applications. *Int. J. Artif. Organs* **2024**, *47*, 356-361, https://doi.org/10.1177/03913988241234548.
6. Derhy, M.; Taha, Y.; Hakkou, R.; Benzaazoua, M. Review of the Main Factors Affecting the Flotation of Phosphate Ores. *Minerals* **2020**, *10*, 1109, https://doi.org/10.3390/min10121109.
7. Lalam, K.; Chhiti, Y.; El Khouakhi, M.; Abidi, A.; Chebak, A. Evaluation and Optimization of Phosphate Recovery from Coarse Rejects Using Reverse Flotation. *Sustainability* **2024**, *16*, 8614, https://doi.org/10.3390/su16198614.
8. Chaikina, M.V.; Bulina, N.V.; Prosanov, I.Y.; Ishchenko, A.V. Formation of Fluorapatite in the Equilibrium System $CaO–P_2O_5–HF–H_2O$ at 298 K in a Nitrogen Atmosphere. *Crystals* **2023**, *13*, 1264, https://doi.org/10.3390/cryst13081264.
9. Montesissa, M.; Sassoni, E.; Boi, M.; Borciani, G.; Boanini, E.; Graziani, G. Synthetic or Natural (Bio-Based) Hydroxyapatite? A Systematic Comparison between Biomimetic Nanostructured Coatings Produced by Ionized Jet Deposition. *Nanomaterials* **2024**, *14*, 1332, https://doi.org/10.3390/nano14161332.
10. García Rodenas, L.; Palacios, J.M.; Apella, M.C.; Morando, P.J.; Blesa, M.A. Surface properties of various powdered hydroxyapatites. *J. Colloid Interface Sci.* **2005**, *290*, 145-154, https://doi.org/10.1016/j.jcis.2005.04.041.
11. White, T.; Ferraris, C.; Kim, J.; Madhavi, S. Apatite – An Adaptive Framework Structure. *Rev. Mineral. Geochem.* **2005**, *57*, 307–401, https://doi.org/10.2138/rmg.2005.57.10.
12. Leroy, N.; Bres, E. Structure and substitutions in fluorapatite. *Eur. Cells Mater.* **2001**, *2*, 36-48.
13. Bazin, T.; Duttine, M.; Julien, I.; Champion, E.; Demourgues, A.; Gaudon, M. Exotic Fe^{II}/Fe^{III} Local Environments in the Hexagonal Channels of Hydroxyapatite. *Inorg. Chem.* **2022**, *61*, 14377-14388, https://doi.org/10.1021/acs.inorgchem.2c02212.
14. Uskoković, V. The role of hydroxyl channel in defining selected physicochemical peculiarities exhibited by hydroxyapatite. *RSC Adv.* **2015**, *5*, 36614-36633, https://doi.org/10.1039/C4RA17180B.
15. da Silva, V.C.; Gomes, D.d.S.; de Medeiros, E.L.G.; Santos, A.M.d.C.; de Lima, I.L.; Rosa, T.P.; Rocha, F.S.; Filice, L.d.S.C.; Neves, G.d.A.; Menezes, R.R. Highly Porous 3D Nanofibrous Scaffold of Polylactic Acid/Polyethylene Glycol/Calcium Phosphate for Bone Regeneration by a Two-Step Solution Blow Spinning (SBS) Facile Route. *Polymers* **2024**, *16*, 3041, https://doi.org/10.3390/polym16213041.
16. Maarouf, F.-E.; Saoiabi, S.; Azzaoui, K.; Khalil, H.; Khalil, M.; El Yahyaoui, A.; Saoiabi, A.; Hammouti, B.; Youssouf, M.H.; Shityakov, S. Amorphous iron phosphate: Inorganic sol-gel synthesis-sodium and potassium insertion. *Indones. J. Sci. Technol.* **2022**, *7*, 187-202, https://doi.org/10.17509/ijost.v7i2.45948.
17. Khalil, H.; Maarouf, F.-E.; Khalil, M.; Saoiabi, S.; Hmamou, M.; Azzaoui, K.; Saoiabi, A.; Ammary, B. The Surface Parameters of a Natural Biosorbent: Giant Reed System. *Biointerface Res. Appl. Chem.* **2023**, *13*, 205, https://doi.org/10.33263/BRIAC133.205.
18. Kosmulski, M. The pH dependent surface charging and points of zero charge. X. Update. *Adv. Colloid Interface Sci.* **2023**, *319*, 102973, https://doi.org/10.1016/j.cis.2023.102973.
19. Hmamou, M.; Maarouf, F.; Ammary, B.; Bellaouchou, A. ADSORPTION OF CITRIC ACID ON IRON (III) HYDROXIDE: MECHANISMS AND STABILITY CONSTANTS OF SURFACE COMPLEXES. *RASĀYAN J. Chem.* **2021**, *14*, 1255-1264, http://dx.doi.org/10.31788/RJC.2021.1426231.

20. Rollin-Martinet, S.; Navrotsky, A.; Champion, E.; Grossin, D.; Drouet, C. Thermodynamic basis for evolution of apatite in calcified tissues. **2013**, *98*, 2037-2045, https://doi.org/10.2138/am.2013.4537.
21. Zhang, L.; Li, Z.; Lu, T.; He, F.; Ye, J. Preparation and properties of porous calcium phosphate ceramic microspheres modified with magnesium phosphate surface coating for bone defect repair. *Ceram. Int.* **2024**, *50*, 7514-7527, https://doi.org/10.1016/j.ceramint.2023.12.055.
22. Fanidi, K.; Bouiahya, K.; Gouza, A.; Saoiabi, A.; Laghzizil, A. Surface properties of Moroccan natural phosphate and its converted hydroxyapatite for adsorption of Cr^{3+}/$Cr_2O_7^{2-}$ ions: Kinetics and isotherms. *Desalin. Water Treat.* **2017**, *100*, 145-150, https://doi.org/10.5004/dwt.2017.21803.
23. Maarouf, F.; Saoiabi, S.; Azzaoui, K.; Chrika, C.; Khalil, H.; Elkaouni, S.; Lhimr, S.; Boubker, O.; Hammouti, B.; Jodeh, S. Statistical optimization of amorphous iron phosphate: inorganic sol–gel synthesis-sodium potential insertion. *BMC Chem.* **2021**, *15*, 48, https://doi.org/10.1186/s13065-021-00774-x.
24. Elyahyaoui, A.; Ellouzi, K.; Al Zabadi, H.; Razzouki, B.; Bouhlassa, S.; Azzaoui, K.; Mejdoubi, E.M.; Hamed, O.; Jodeh, S.; Lamhamdi, A. Adsorption of Chromium (VI) on Calcium Phosphate: Mechanisms and Stability Constants of Surface Complexes. *Appl. Sci.* **2017**, *7*, 222, https://doi.org/10.3390/app7030222.
25. Oliveira, P.d.; Mansur, H.; Mansur, A.; Silva, G.d.; Clark Peres, A.E. Apatite flotation using pataua palm tree oil as collector. *J. Mater. Res. Technol.* **2019**, *8*, 4612-4619, https://doi.org/10.1016/j.jmrt.2019.08.005.
26. Yu, L.; Yu, P.; Bai, S. A Critical Review on the Flotation Reagents for Phosphate Ore Beneficiation. *Minerals* **2024**, *14*, 828, https://doi.org/10.3390/min14080828.
27. Lasota, A.; Gorzelak, M.; Turżańska, K.; Kłapeć, W.; Jarzębski, M.; Blicharski, T.; Pawlicz, J.; Wieruszewski, M.; Jabłoński, M.; Kuczumow, A. The Ways of Forming and the Erosion/Decay/Aging of Bioapatites in the Context of the Reversibility of Apatites. *Int. J. Mol. Sci.* **2024**, *25*, 11297, https://doi.org/10.3390/ijms252011297.
28. Yang, Y.-W.; Yang, J.-C. Characterization of calcium phosphate as a gene carrier (I): Electrochemical properties. *Drug Deliv.* **1996**, *3*, 173–179, https://doi.org/10.3109/10717549609029447.
29. Sposito, G. The Chemistry of Soils, 1st Edition. Oxford University Press: Oxford, New York, **1989**; https://doi.org/10.1017/S0016756800014059.
30. Lafhaj, Z.; Filippov, L.O.; Filippova, I.V. Improvement of calcium mineral separation contrast using anionic reagents: electrokinetics properties and flotation. *J. Phys.: Conf. Ser.* **2017**, *879*, 012012, https://doi.org/10.1088/1742-6596/879/1/012012.
31. Watanabe, H.; Seto, J. The Point of Zero Charge and the Isoelectric Point of γ-Fe_2O_3 and α-Fe_2O_3. *Bull. Chem. Soc. Jpn.* **1986**, *59*, 2683–2687, https://doi.org/10.1246/bcsj.59.2683.
32. Cristiano, E.; Hu, Y.-J.; Sigfried, M.; Kaplan, D.; Nitsche, H. A Comparison of Point of Zero Charge Measurement Methodology. *Clays Clay Miner.* **2011**, *59*, 107-115, https://doi.org/10.1346/CCMN.2011.0590201.
33. Tan, W.-f.; Lu, S.-j.; Liu, F.; Feng, X.-h.; He, J.-z.; Koopal, L.K. DETERMINATION OF THE POINT-OF-ZERO CHARGE OF MANGANESE OXIDES WITH DIFFERENT METHODS INCLUDING AN IMPROVED SALT TITRATION METHOD. *Soil Sci.* **2008**, *173*, 277-286, https://doi.org/10.1097/SS.0b013e31816d1f12.
34. Menéndez, J.A.; Illán-Gómez, M.J.; y León, C.A.L.; Radovic, L.R. On the difference between the isoelectric point and the point of zero charge of carbons. *Carbon* **1995**, *33*, 1655-1657, https://doi.org/10.1016/0008-6223(95)96817-R.
35. Sahai, N.; Kaddour, H.; Dalai, P.; Wang, Z.; Bass, G.; Gao, M. Mineral Surface Chemistry and Nanoparticle-aggregation Control Membrane Self-Assembly. *Sci. Rep.* **2017**, *7*, 43418, https://doi.org/10.1038/srep43418.
36. Leiviskä, T.; Gehör, S.; Eijärvi, E.; Sarpola, A.; Tanskanen, J. Characteristics and potential applications of coarse clay fractions from Puolanka, Finland. *Cent. Eur. J. Eng.* **2012**, *2*, 239-247, https://doi.org/10.2478/s13531-011-0067-9.
37. Alexandrino, J.S.; Peres, A.E.C.; Lopes, G.M.; Rodrigues, O.M.S. Dispersion degree and zeta potential of hematite. *Rem: Rev. Esc. Minas* **2016**, *69*, 193-198, https://doi.org/10.1590/0370-44672014690073.
38. Ciobanu, G.; Harja, M. STUDIES ON THE SORPTION OF LEVOFLOXACIN FROM AQUEOUS SOLUTIONS ONTO NANOHYDROXYAPATITE. *Rev. Roum. Chim.* **2018**, *63*, 593-601.
39. Akartasse, N.; Azzaoui, K.; Mejdoubi, E.; Hammouti, B.; Elansari, L.L.; Abou-salama, M.; Aaddouz, M.; Sabbahi, R.; Rhazi, L.; Siaj, M. Environmental-Friendly Adsorbent Composite Based on Hydroxyapatite/Hydroxypropyl Methyl-Cellulose for Removal of Cationic Dyes from an Aqueous Solution. *Polymers* **2022**, *14*, 2147, https://doi.org/10.3390/polym14112147.

40. Perrone, J.; Fourest, B.; Giffaut, E. Surface Characterization of Synthetic and Mineral Carbonate Fluoroapatites. *J. Colloid Interface Sci.* **2002**, *249*, 441–452, https://doi.org/10.1006/jcis.2002.8255.
41. Inagaki, T.; Takenaka, N.; Nagaoka, M. The crucial role of electron transfer from interfacial molecules in the negative potential shift of Au electrode immersed in ionic liquids. *Phys. Chem. Chem. Phys.* **2018**, *20*, 29362-29373, https://doi.org/10.1039/c8cp04594a.
42. Tripkovic, V.; Björketun, M.E.; Skúlason, E.; Rossmeisl, J. Standard hydrogen electrode and potential of zero charge in density functional calculations. *Phys. Rev. B* **2011**, *84*, 115452, https://doi.org/10.1103/PhysRevB.84.115452.
43. Zahn, D.; Hochrein, O. Computational study of interfaces between hydroxyapatite and water. *Phys. Chem. Chem. Phys.* **2003**, *5*, 4004-4007, https://doi.org/10.1039/B306358E.
44. Jinnouchi, R.; Anderson, A.B. Electronic structure calculations of liquid-solid interfaces: Combination of density functional theory and modified Poisson-Boltzmann theory. *Phys. Rev. B* **2008**, *77*, 245417, https://doi.org/10.1103/PhysRevB.77.245417.
45. Chaabouni, A.; Chtara, C.; Nzihou, A.; El Feki, H. Study the Nature and the Effects of the Impurities of Phosphate Rock in the Plants of Production of Phosphoric Acid. *J. Adv. Chem.* **2014**, *7*, 1296-1299, https://doi.org/10.24297/jac.v7i2.5560.
46. Hakkou, R.; Benzaazoua, M.; Bussière, B. Valorization of Phosphate Waste Rocks and Sludge from the Moroccan Phosphate Mines: Challenges and Perspectives. *Procedia Eng.* **2016**, *138*, 110-118, https://doi.org/10.1016/j.proeng.2016.02.068.
47. Amankonah, J.O.; Somasundaran, P. Effects of dissolved mineral species on the electrokinetic behavior of calcite and apatite. *Colloids Surf.* **1985**, *15*, 335-353, https://doi.org/10.1016/0166-6622(85)80082-2.
48. Wang, G. Ionic stability of oxide particles in polar organic media. *American Mineralogist*, **2011**, **96**(3–4), 191–199. https://doi.org/10.2138/am.2011.3738
49. Nassar, M.Y.; Ahmed, I.S.; Mohamed, T.Y.; Khatab, M. A controlled, template-free, and hydrothermal synthesis route to sphere-like α-Fe_2O_3 nanostructures for textile dye removal. *RSC Adv.* **2016**, *6*, 20001-20013, https://doi.org/10.1039/C5RA26112K.
50. Nduwa-Mushidi, J.; Anderson, C.G. Surface Chemistry and Flotation Behaviors of Monazite–Apatite–Ilmenite–Quartz–Rutile–Zircon with Octanohydroxamic Acid. *J. Sustain. Metall.* **2017**, *3*, 62–72, https://doi.org/10.1007/s40831-016-0114-0.
51. Ahmed, Z.; Wu, P.; Xu, Y.; Keerio, H.A.; Wu, J.; Ye, Q.; Niu, W.; Chen, M.; Dang, Z. Enhanced Single and Simultaneous As(III) Adsorption in Pearl River Delta Water by Hexylamine Functionalized Vermiculite. *Water* **2021**, *13*, 2412, https://doi.org/10.3390/w13172412.
52. Kim, S.; Palomino, A.M. Polyacrylamide-treated kaolin: A fabric study. *Appl. Clay Sci.* **2009**, *45*, 270-279, https://doi.org/10.1016/j.clay.2009.06.009.
53. Alvarez-Silva, M.; Uribe-Salas, A.; Mirnezami, M.; Finch, J.A. The point of zero charge of phyllosilicate minerals using the Mular–Roberts titration technique. *Miner. Eng.* **2010**, *23*, 383-389, https://doi.org/10.1016/j.mineng.2009.11.013.
54. Chernyshova, I.V.; Ponnurangam, S.; Somasundaran, P. Effect of nanosize on catalytic properties of ferric (hydr)oxides in water: Mechanistic insights. *J. Catal.* **2011**, *282*, 25-34, https://doi.org/10.1016/j.jcat.2011.05.021.
55. Singh, S. S. The formation and coexistence of gibbsite, boehmite, alumina and alunite at room temperature. Canadian Journal of Soil Science, **1982**, **62**, 327–332. https://doi.org/10.4141/cjss82-036
56. Ardizzone, S.; Bianchi, C.L.; Vercelli, B. Acid/base and surface features of pure phase magnesia powders. *Colloids Surf. A: Physicochem. Eng. Asp.* **1998**, *144*, 9-17, https://doi.org/10.1016/S0927-7757(98)00518-4.
57. Markley, T.; Dligatch, S.; Trinchi, A.; Muster, T.H.; Bendavid, A.; Martin, P.; Lau, D.; Bradbury, A.; Furman, S.; Cole, I.S. Multilayered coatings: Tuneable protection for metals. *Corros. Sci.* **2010**, *52*, 3847-3850, https://doi.org/10.1016/j.corsci.2010.07.028.
58. Wang, B.; Xiong, X.; Ren, H.; Huang, Z. Preparation of MgO nanocrystals and catalytic mechanism on phenol ozonation. *RSC Adv.* **2017**, *7*, 43464-43473, https://doi.org/10.1039/C7RA07553G.
59. Naeimeh, G.T. Surface-chemical interactions between apatite and hematite in aqueous suspensions. Doctoral Thesis, University of British Columbia, Vancouver, Canada, **2020**, https://doi.org/10.14288/1.0388358.
60. Sondi, I. (**2018**). Flotation. In: Drioli, E., Giorno, L. (eds) *Encyclopedia of Membranes*. Springer. https://doi.org/10.1007/978-3-319-95022-8_245

61. Janusz W., Skwarek E., Żarko V. I., Gun'ko V. M. (**2007**). Structure of electrical double layer at the Al_2O_3-SiO_2/electrolyte solution interface. *Physicochemical Problems of Mineral Processing*, 41, 215–225.
62. Owens, C.L.; Nash, G.R.; Hadler, K.; Fitzpatrick, R.S.; Anderson, C.G.; Wall, F. Apatite enrichment by rare earth elements: A review of the effects of surface properties. *Adv. Colloid Interface Sci.* **2019**, *265*, 14-28, https://doi.org/10.1016/j.cis.2019.01.004.
63. Skwarek, E. Adsorption of Cs^+ at the Hydroxyapatite/Aqueous Electrolyte Interface. *Adsorp. Sci. Technol.* **2015**, *33*, 575-580, https://doi.org/10.1260/0263-6174.33.6-8.575.
64. Cristiano, E.; Hu, Y.-J.; Siegfried, M.; Kaplan, D.; Nitsche, H. A Comparison of Point of Zero Charge Measurement Methodology. *Clays Clay Miner.* **2011**, *59*, 107–115. https://doi.org/10.1346/CCMN.2011.0590201.

Publisher's Note & Disclaimer